ETH zürich

ETH Library

On the variability of the site-response parameters of the active rock slope in Brienz/Brinzauls (Switzerland)

Journal Article

Author(s):
Borgeat, Xavier; Glueer, Franziska; Häusler, Mauro; Hobiger, Manuel; Fäh, Donat

Publication date:
2025-01

Permanent link:
https://doi.org/10.3929/ethz-b-000716692

Rights / license:
Creative Commons Attribution 4.0 International

Originally published in:
Geophysical Journal International 240(1), https://doi.org/10.1093/gji/ggae412

Funding acknowledgement:
177586 - 4D seismic response and slope failure (SNF)
214916 - Quantification of the seismic response of instable slopes and its time variability: an important indicator for potential mass movements (SNF)

This page was generated automatically upon download from the ETH Zurich Research Collection.
For more information, please consult the Terms of use.

Geophysical Journal International

Geophys. J. Int. (2025) **240,** 779–790
Advance Access publication 2024 November 19
GJI Seismology

https://doi.org/10.1093/gji/ggae412

On the variability of the site-response parameters of the active rock slope in Brienz/Brinzauls (Switzerland)

X. Borgeat [1], F. Glueer [1], M. Häusler [1], M. Hobiger [2] and D. Fäh [1]

[1] *Swiss Seismological Service, Department of Earth and Planetary Sciences, ETH Zurich,* CH-8092 *Zurich, Switzerland. E-mail: xavier.borgeat@eaps.ethz.ch*
[2] *Federal Institute for Geosciences and Natural Resources (BGR), Earthquakes and Geo-Hazard Assessment,* D-30655 *Hannover, Germany*

Accepted 2024 November 12. Received 2024 October 23; in original form 2024 June 13

SUMMARY

Unstable rock slopes, prone to collapse, pose an increasingly severe threat to both people and infrastructures, necessitating effective monitoring for risk mitigation. While many techniques rely on surface displacements to assess slope stability, seismic indicators such as resonance frequency, variations in seismic wave velocity and site amplification offer valuable insights into the structural integrity of the slope, aspects not captured by surface deformation alone. Research has demonstrated that these site-response parameters can serve as monitoring tools to detect precursory signs of failure, such as a drop in resonance frequency and relative seismic wave velocity prior to collapse. Still, environmental factors like temperature, precipitation, snow melt, earthquakes and freeze-thaw cycles transiently influence the seismic response. Our main objective is to understand the correlations and drivers between environmental parameters and seismic response, distinguishing between reversible and irreversible changes in dynamic behaviour. Over a 5-yr monitoring period, we continuously recorded ambient vibration data at the Brienz/Brinzauls instability and monitored three different site-response parameters (resonance frequency, site amplification, relative seismic wave velocity variation) using enhanced frequency domain decomposition, site-to-reference spectral ratio and single station ambient vibrations correlation techniques. Our results highlight a long-term increase in site amplification and a long-term decrease in first and second resonance frequencies, indicating ongoing structural weakening. Temperature was found to correlate with seasonal variations of seismic wave velocity with a few day's time lag. Snow melting and rainfalls exerted a secondary influence, temporarily reducing relative seismic wave velocity during snowmelt and rainfall. Our findings suggest that single-station relative seismic velocity variations are mainly influenced by the shallow subsurface (depth of about 30 m), limiting its application to study the stability this deep structure.

Key words: Instability analysis; Seismic interferometry; Seismic noise; Site effects.

1 INTRODUCTION

Natural risks such as avalanches, flooding, earthquakes or mass movements pose ongoing dangers to the population and infrastructure. Some unstable slopes are on the verge of collapsing or accelerating towards a catastrophic failure and represent real socio-economic threats. In 2020, a report by Confédération Suisse (2020) indicated that this hazard will likely increase due to global warming. Early detection and continuous monitoring of unstable slopes are crucial for effectively mitigating the associated risks.

Numerous techniques are available for monitoring and identifying unstable slopes. One approach involves monitoring surface deformations using methods like Global Navigation Satellite System (GNSS), total station monitoring with reflectors/prisms (TPS), synthetic aperture radar interferometry (InSAR), light detection and ranging (LiDAR) or mechanical sensors (e.g. extensometers). Another approach is the detection of internal changes of the instability, such as alterations in material stiffness, through recordings of ambient vibrations, even when surface deformations are absent (Lévy *et al.* 2010; Larose *et al.* 2015; Bottelin *et al.* 2017; Burjánek *et al.* 2018; Kleinbrod *et al.* 2019; Bontemps *et al.* 2020; Fiolleau *et al.* 2020; Colombero *et al.* 2021; Häusler *et al.* 2021; Le Breton *et al.* 2021; Bessette-Kirton *et al.* 2022; Geimer *et al.* 2022). Tracking different site-response parameters such as resonance frequency (e.g. Lévy *et al.* 2010), relative changes in seismic wave velocity (e.g. Le Breton *et al.* 2021), rate of microseismic frequency (e.g. Amitrano *et al.* 2007) and site amplification (e.g. Häusler *et al.* 2022) have been proposed as monitoring and/or potential early warning tools. However, as discussed in the review paper of Le Breton *et al.*

© The Author(s) 2024. Published by Oxford University Press on behalf of The Royal Astronomical Society. This is an Open Access article distributed under the terms of the Creative Commons Attribution License (https://creativecommons.org/licenses/by/4.0/), which permits unrestricted reuse, distribution, and reproduction in any medium, provided the original work is properly cited.

Downloaded from https://academic.oup.com/gji/article/240/1/779/7905064 by Milak user on 17 January 2025

(2021) on seismic wave velocity variation, the role of environmental parameters on site-response parameters remains to be fully understood. Environmental factors like rainfall, snow melting and temperature fluctuations can lead to notable reversible alterations in site-response parameters. Consequently, implementing an early warning system becomes challenging, as discerning variations induced by these environmental parameters from signs of failure is not straightforward. It has been shown that resonance frequency was positively correlated with temperature (e.g. Lévy *et al.* 2010; Bottelin *et al.* 2013a; Burjánek *et al.* 2018; Häusler 2021; Geimer *et al.* 2022) and negatively correlated with water input through precipitation and snow melting (e.g. Häusler *et al.* 2021). Site amplification was correlated with rainfall (e.g. Häusler *et al.* 2022). Variations in seismic wave velocity due to environmental parameters were highlighted in different studies, with factors depending on rainfalls (e.g. Hillers *et al.* 2014; Obermann *et al.* 2014; De Plaen *et al.* 2016; Bontemps *et al.* 2020), barometric pressure (e.g. Niu *et al.* 2008), temperature (e.g. Richter *et al.* 2014; Hillers *et al.* 2015), groundwater table (e.g. Meier *et al.* 2010; Voisin *et al.* 2016), freeze/thaw cycles (e.g. Guillemot *et al.* 2020) and/or earthquakes (e.g. Hobiger *et al.* 2014; Bontemps *et al.* 2020) influencing the seismic velocity.

Repeated temperature fluctuations, rainfalls and earthquakes can induce slope damage, increasing its vulnerability over time (Finlayson & Statham 1980; Julian & Anthony 1996; Gunzburger *et al.* 2005). While previous research acknowledges reversible seasonal variations in site-response parameters linked to environmental factors, the identification of gradual damage accumulation has been limited to hours/days preceding a failure (e.g. Lévy *et al.* 2010; Mainsant *et al.* 2012; Bertello *et al.* 2018; Fiolleau *et al.* 2020).

The active rock slope instability at Brienz/Brinzauls, located in the Canton of Grisons, Switzerland, presents a unique opportunity to analyse and quantify the time variability of various site response parameters, thanks to an extended monitoring period of five years. Previous research by Häusler *et al.* (2022) documented 30 months of monitoring data, including wavefield polarization, absolute site amplification and displacement field, alongside geophysical mapping using array measurements. In a more recent study, Häusler *et al.* (2024) updated the previous survey by additionally tracking resonance frequency and seismic events. They discussed the observed changes before, during and after a partial collapse in June 2023. Both studies monitored a fast-moving subdomain in the upper part of the instability using a single seismic station.

In this study, we use the data from a second seismic station located in the village of Brienz/Brinzauls to calculate site amplification using site-to-reference spectral ratio (SRSR) and track relative seismic velocity variations (dv/v) using cross-correlation of ambient vibrations between the two stations. As in Häusler *et al.* (2024), we study the resonance frequency of the upper subdomain, utilizing enhanced frequency domain decomposition (EFDD). However, while the earlier study focused mainly on seismic signals and hydrological factors (discharge of the Albula river and precipitation), we also use temperature data to understand how environmental factors influence site-response parameters, intending to distinguish between reversible and irreversible variations in site-response parameters due to environmental drivers. While past studies have monitored relative seismic wave velocity variations and resonance frequency (e.g. Colombero *et al.* 2018; Valentin 2018), only a few studies monitored site amplification. In this study, after discussing the site and methods, we compare the time variability of three site-response parameters (relative seismic velocity variations, resonance frequency and relative amplification) with environmental and kinematic parameters such as temperature, precipitation, snow depth, river discharge and surface displacement rate. This study shows seismic signatures of a gradual accumulation of damage to the rock slope, evidenced by a linear decrease in resonance frequency alongside increased site amplification. Additionally, our findings suggest that relative seismic velocity variations observed at a single station may primarily reflect changes in the shallow subsurface rather than the response of the entire instability.

2 THE BRIENZ/BRINZAULS ROCK SLOPE INSTABILITY

The village of Brienz/Brinzauls is located in the canton of Grisons in Switzerland, within the municipality of Albula/Alvra. The village is located on a deep-seated gravitational slope deformation known for many years (e.g. Heim 1932). At present, the instability spans an area exceeding 10 km^2 (Krähenbühl & Nänni 2017), with the Albula River marking the lower limit of the instability. Fig. 1(a) shows a photo of the instability and the location within Switzerland. Between 2018 and 2021, several boreholes were drilled. The instability can be divided into two interlinked parts. The lower part (called 'Rutschung-Dorf'), where the village is located, exhibits primarily slow sliding movements ($\sim 1\ m\,yr^{-1}$) with relatively low slope inclination ($\sim 10°$), with a lithology mainly composed of Flysch, with an exception beneath the village where schists from the Allgäu formation (secondary deposits) overlay the Flysch (BTG (Büro für Technische Geologie AG), 2021). The sliding plane reaches approximately 150 m in the village. Following the seismic classification of Kleinbrod *et al.* (2017), this part can be classified as a depth-controlled site, that is, the ambient vibrations are controlled by horizontal surface wave propagation and the depth-dependent shear wave velocity profile.

The upper part (called 'Rutschung Berg') involves sliding, toppling and falling, with significantly higher slope inclination (between 35 and 55°). The lithology includes Allgäu formation (schists), Raibler layers (Dolomite and Rauwacke) and heavily fractured Arlberg Dolomite. The sliding plane is found at shallower depths (60–80 m), while the water table is approximately 300 m deep at the top of the instability (Figi *et al.* 2022). The seismic station BRIZ2, located on a relatively flat part of the upper instability (named 'Plateau'), sits on Arlberg Dolomite. A simplified map of the site lithology based on BTG (Büro für Technische Geologie AG) (2021) is shown in Fig. 1(b). The upper part can be seismically classified as a volume-controlled site with normal mode behaviour (eigenvibrations). Deep open fractures divide the deep-seated instability into several blocks acting as resonators and create amplified ground motion perpendicular to open fractures over a short frequency band around the resonance frequency of 2.8 Hz.

The initiation of mass movement can be traced back to prehistoric times, likely due to the glacial retreat following the last glacial maximum. Historical records indicate recurring landslides in the region, including the 'Igl Rutsch' event in 1878, which displaced approximately $2.5 \times 10^6\ m^3$ of material nearly reaching the village of Brienz/Brinzauls (Heim 1932; Krähenbühl & Nänni 2017). Heim (1932) noted that dry periods correlated with a deceleration of movement, while moist periods accelerated it. Since 1921, displacement rates have been monitored. From 1921 to 2000, relatively

Downloaded from https://academic.oup.com/gji/article/240/1/779/7905064 by Milak user on 17 January 2025

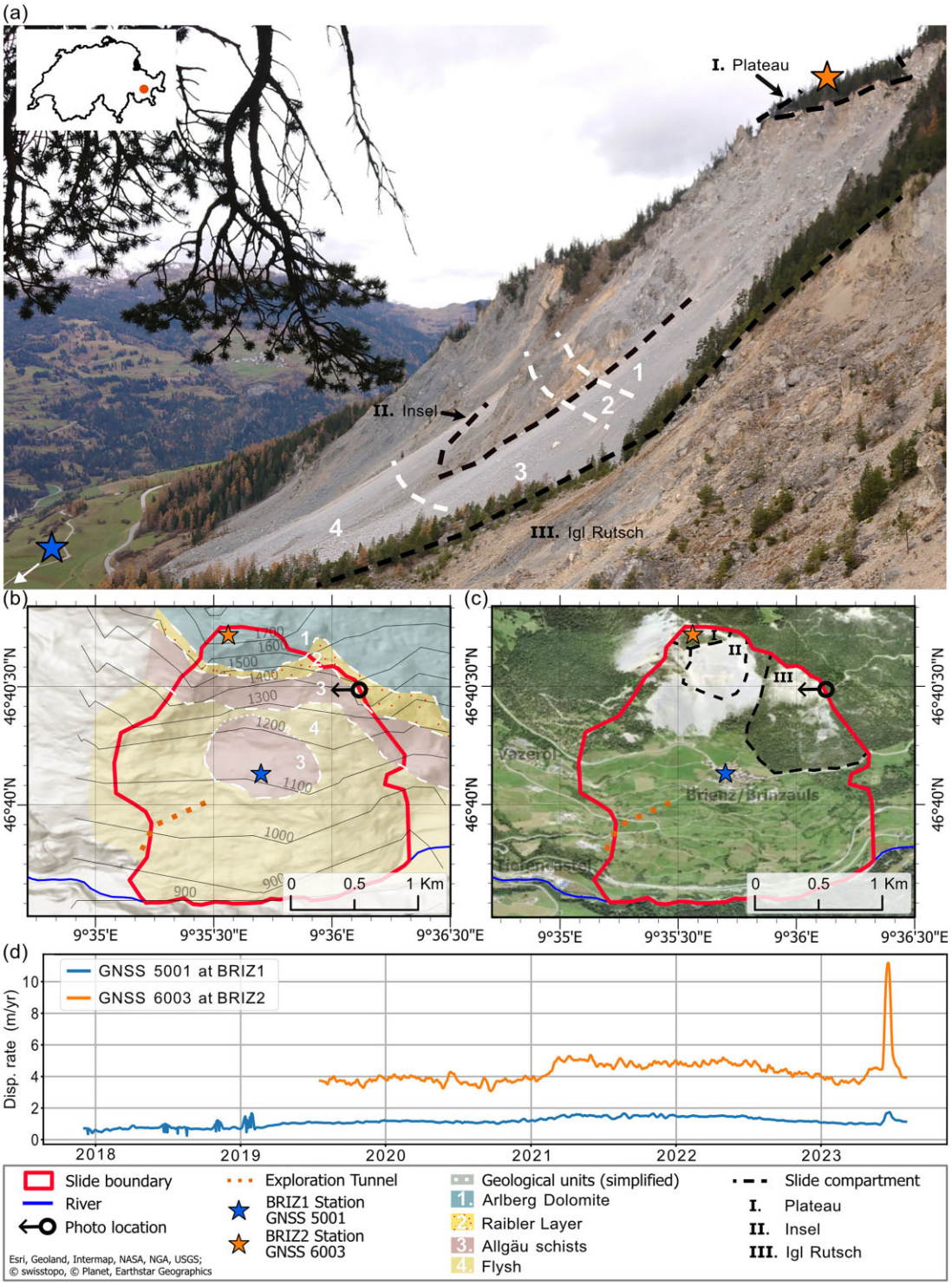


Figure 1. Visualizing the site of Brienz/Brinzauls. (a) Photo of the instability (from 2022 November 15). The top left map shows the location of the site in Switzerland. (b) shows a simplified map of the lithologies (BTG (Büro für Technische Geologie AG), 2021). The contour lines are based on swissALTI3D data (www.swisstopo.ch). (c) shows the location of different compartments. (d) shows the displacement rate of the instability. The results for GNSS station 5001 suffer from substantial noise during the first 1.5 yr.

slow displacement rates were observed (0.05–0.1 m yr^{-1}). In 2010, the instability accelerated with velocities around 1 m yr^{-1} at the village and 4–5 m yr^{-1} at the top. After recognizing the acceleration in 2010, several remediation measures were applied (e.g. constructing an exploratory tunnel in 2020; Figs 1(c) and (d)). A compartment above the village of Brienz/Brinzauls collapsed on 2023 June 15, releasing a volume of $\sim 1.2 \times 10^6$ m^3 (Loew *et al.* 2023). This compartment, named 'Insel', is located between the instability's lower

Downloaded from https://academic.oup.com/gji/article/240/1/779/7905064 by Mlak user on 17 January 2025

and upper part and is made from Allgäu formation, Raibler layers and Arlberg Dolomite. The 3-D displacement rates for the upper and lower part of the instability are shown in Fig. 1(d).

Various geophysical surveys were conducted in the area: at the top of the instability, an array-based seismological mapping was performed first by Kleinbrod *et al.* (2019) and in more detail by Häusler *et al.* (2022). BTG (Büro für Technische Geologie AG) (2021) developed a geologic–kinematic model based on displacements, geoelectric and active seismic measurements, boreholes and deformation analyses. Recently, Schneider *et al.* (2023) studied the time-variability of rock-falls of this instability recorded from a Doppler radar system.

3 MATERIALS AND METHODS

3.1 Data acquisition

The site is equipped with two buried three-components 1 s Lennartz seismic sensors with Nanometrics Centaur digitizers sampling at 200 Hz. Station BRIZ2, located on the upper subdomain of the instability on a relatively flat area (named 'Plateau'), was installed in early June 2018. The reference station BRIZ1 is located in the middle of the village of Brienz/Brinzauls. This velocimeter, replacing a previously installed strong-motion sensor, was installed in late November 2020 (Swiss Seismological Service (SED) at ETH Zurich, 2012). The amplification functions, obtained at the seismic stations BRIZ1 and BRIZ2 with empirical spectral modelling (ESM; Edwards *et al.* 2013) from earthquake data, are shown in Fig. S1 of Supporting Information. For station BRIZ1, located on the lower part of the instability, one main resonance frequency at low frequency ($\sim$ 1.6 Hz) can be identified (see Fig. S1(a) of Supporting Information). Above 2 Hz, the frequencies are not strongly amplified compared to the Swiss reference rock profile. Several resonance frequencies can be identified in the amplification functions from ESM for station BRIZ2 (one around 1.8 Hz and a second around 2.8 Hz). The amplifications at BRIZ2 are larger than at BRIZ1 (see Fig. S1(b) of Supporting Information). We focused our analysis on two frequency bands, containing the fundamental resonance frequency (f1: 1.6–2.3 Hz) and second resonance frequency (f2: 2.3–3.05 Hz). Passive seismic mapping suggests that the first resonance frequency is sensitive to a large instability with an estimated volume of 10–25 $\times$ 10^6 m^3 with unresolved spatial extent (Häusler *et al.* 2022). The second resonance frequency depends on a subvolume around the seismic station BRIZ2 with an estimated volume of 1–2 $\times$ 10^6 m^3. The spatial extent of this subvolume is shown in Figs 3(b) and 4(c) of Häusler *et al.* (2022).

A meteorological station from Holfuy was colocated with BRIZ2. The data provided by the meteorological station are soil and air temperature, wind speed, direction and gust speed, air humidity, precipitation, solar radiation, barometric pressure and soil moisture. For this study, we used temperature (in °C), wind speed (in km h^{-1}) and precipitation (in mm). We used temperature and precipitation recordings from a nearby weather station operated by the Swiss Federal Office for Meteorology and Climatology (www.meteoswiss.ch), which is located in Valbella (station VAB), to assess the quality of the Holfuy station primarily and to complete the meteorological data sets (the Holfuy station was installed after the seismic sensor BRIZ2). Comparison using the Pearson correlation coefficient (Cohen *et al.* 2009) revealed that the data collected at the Holfuy station closely align with those recorded by Meteo Schweiz (Pearson correlation coefficient of 0.97 for temperature and 0.91 for precipitation index).

A hydrological station operated by the Federal Office for the Environment (FOEN) in Tiefencastel (station 2141) recorded the discharge of the Albula river, which marks the lower limit of the instability. Two global navigation satellite system (GNSS) stations (GNSS 6001 and 5003) were located close to the two seismic sensors (data acquired from the Office for Forest and Natural Hazards, Canton of Grisons). We retrieved the daily displacement rate from the GNSS points' coordinates. Lastly, we acquired snow height data from a station in Lenzerheide (station ROT3) operated by the SLF Institute for Snow and Avalanche Research (data from Intercantonal Measurement and Information System IMIS (2023)). Fig. S2 of Supporting Information provides a map showing the sensor locations, and Table S1 of Supporting Information lists their corresponding coordinates. We applied the precipitation index P_c by Helmstetter & Garambois (2010) to better represent the contribution of the groundwater storage capacity. The Index accounts for the sum of daily precipitation with a weight decaying exponentially for previous daily precipitation and is defined as

$$P_c(t_i) = \sum_{j=0}^{i} P(t_j)\ \exp\left(-\frac{t_i - t_j}{t_c}\right), \tag{1}$$

where P_c is the cumulative precipitation index at time t_i, $P(t_j)$ is the daily precipitation at time t_j and t_c is the characteristic time, set to 14 d. As in Häusler *et al.* (2022), we used the normalized precipitation index in this work, normalizing the precipitation index as follows

$$P_c(t_i) = \frac{\sum_{j=0}^{i} P(t_j)\ \exp\left(-\frac{t_i - t_j}{t_c}\right)}{\sum_{j=0}^{i} \exp\left(-\frac{t_i - t_j}{t_c}\right)}. \tag{2}$$

3.2 Site amplification from site-to-reference spectral ratio (SRSR)

To obtain the seismic amplification based on the site-to-reference spectral ratio (SRSR; Borcherdt 1970; Perron *et al.* 2018), the ambient vibration data are first pre-processed by removing the polynomial trend and the mean, and by removing the instrumental response. Then, the power spectra are calculated hourly using the multitaper spectral method from Prieto *et al.* (2009). This method involves taking the ratio of the Fourier spectra of the two stations for each component within time windows of 100 s. The output provides the mean and standard deviation of the calculated power spectra for frequencies ranging from 1 to 10 Hz. The SRSRs were obtained by taking the ratio of the geometrical mean of the horizontal components of station BRIZ2 and using BRIZ1 as the reference station.

It is assumed that the sources of ambient vibrations are far away compared to the interstation distance. This ensures that the observed amplification is primarily due to local effects, with source and path effects considered identical at both stations. To mitigate any disturbances from daily anthropogenic noise sources, the SRSRs were only calculated from 0 to 5 am UTC at night because the reference station was located in the village of Brienz/Brinzauls. Additionally, SRSRs calculated when wind velocity exceeded 5 km h^{-1} were not considered as initial findings showed a strong correlation between amplification and wind velocity. Site amplification depends on topography, impedance contrast with surrounding bedrock and

Downloaded from https://academic.oup.com/gji/article/240/1/779/7905064 by Milak user on 17 January 2025

internal fractures (Gischig *et al.* 2015). While the first two are nearly constant, the third is related to instability stiffness. An increase in fracture width, depth and/or fracture contact stiffness will lead to an increase in site amplification.

3.3 Relative seismic wave velocity variation from single-station cross-correlation

The method consists of cross-correlating different seismic components of a single seismic station, with one component treated as the virtual source and the other as the virtual receiver, an approach with a similar workflow as in Hobiger *et al.* (2014). By computing hourly cross-correlations for six-component configurations (EN, NZ, ZE for positive and negative times) and stacking the results daily for stability, it became possible to identify waves travelling through the medium and being captured by another component, arriving with a similar lag each day. The slight variations in these stable phases were attributed to changes in the material properties surrounding the seismic station, which might primarily be due to alterations in the medium's stiffness.

The sum of all daily cross-correlation functions (ccf) was defined as reference ccf. To obtain the relative variation in seismic wave velocity, we compared daily ccf and stretched versions of reference ccf for a specific window in the coda part. Correlograms and their corresponding reference cross-correlation functions are given in Figs S3 and S4 of Supporting Information. The dashed white lines show the time window considered, defined after direct waves arrive. We set the lower limit to 2.2 s and we consider a length of 10 periods based on the upper frequency (window from 2.2 to 6.55 s for the first frequency band (1.6–2.3 Hz) and from 2.2–5.48 s for the second frequency band (2.3–3.05 Hz)). For all six configurations (three-component combinations times two directions of travelling waves), we recorded the stretching factor (Δ), constrained to be within ± 3 per cent and the cross-correlation coefficients best matching the two-time series, serving as a quality factor. Assuming that the medium changes are homogeneous around the sensor, the stretching factor Δ equals the relative changes in velocity. A weighted average of the six component configurations was taken to increase the method's stability.

We also computed standard ambient vibration interferometry using the two seismic stations with the MSNoise code from Lecocq *et al.* (2014). Similar results were found with the single-station ambient vibration interferometry. As single-station methods had a longer time series, we focused our analysis on the results of this method.

3.4 Resonance frequency tracking using enhanced frequency domain decomposition (EFDD)

We tracked the first two resonance frequencies applying the enhanced EFDD method from Brincker *et al.* (2001). This method was widely applied in different civil engineering projects (e.g. Kasımzade *et al.* 2019), and to analyse different slope instabilities (e.g. Bottelin *et al.* 2013b; Häusler *et al.* 2019). EFDD retrieves the resonance frequency and the modal shapes by applying a singular value decomposition (SVD) of the cross-power-spectral density (CPSD). More details are given in Häusler *et al.* (2021). Hourly values of resonance frequencies are retrieved using an automatic procedure as described in Häusler *et al.* (2024). As for shear wave velocity, the fundamental frequency is proportional to the structure's stiffness (Chen & Lui 2005; Jia *et al.* 2021, 2022).

4 RESULTS

4.1 Site-to-reference spectral ratio (SRSR)

The site-to-reference spectral ratio (SRSR) was tracked for 2.5 yr. Fig. 2(a) depicts the probability density function of the daily relative amplification with mean and standard deviation plotted in grey. Relative amplification values span between 1.5 and 6, with a mean value of around 2–2.5. As frequency increases, amplification exhibits higher values and variability. Fig. 2(b) shows the spectrogram of the geometric mean amplification and reveals a constant amplification over time apart from a decrease in amplification for frequencies higher than 8 Hz post-2021. After April 2023 (depicted by the first vertical dashed line in Fig. 2(b)), a pronounced amplification extends across the entire frequency range for several weeks until the 15th of June (marked by a second vertical dashed line), the day of failure. This amplification is likely associated with the moving 'Insel' acting as a source of ambient vibrations. During this time, source and path effects are not the same. Hence, we have removed this period from the time series for more rigorous analysis, so, in panels (c)–(f), the time-series span until the end of April 2023.

In Figs 2(c) and (d), the time series depict the median amplification for the frequency bands from 1.6 to 2.3 Hz and from 2.3 to 3.05 Hz, respectively. The dashed lines represent the long-term evolution of the amplification. Long-term trends are obtained using a locally weighted linear regression using a locally estimated scatterplot smoothing (LOESS method; Cleveland 1979). The amplification in Fig. 2(c) exhibits a consistent increase with no discernible seasonal variations over the years. Occasional transient decreases or increases can be observed. The site amplification for the second frequency band shows an increase until early 2022 and remains constant after that (Fig. 2(d)).

Fig. 2(e) shows temperature, precipitation index and river discharge. Some spikes in the site amplification correlate with spikes in Albula discharge (some local maxima of the discharge are marked with vertical dashed lines). For the first frequency band, not all discharge spikes lead to an increase in site amplification. The correlation is better for the second frequency band. Although the times of the spikes in discharge and amplification match, the amplitude does not. For example, in October 2022, a substantial increase in site amplification can be observed, while the discharge spike is relatively low. In summer 2021, despite the relatively large spike of discharge, the site amplification remains lower than in October 2022. Some spikes in amplification are not related to hydrological factors. So, although there is a matching between discharge and amplification, the site-response variations remain hardly predictable from environmental parameters. The kinematic of the instability (displacement rate shown in Fig. 2(f)) does neither appear to be correlated with site amplification nor with environmental parameters.

4.2 Seismic wave velocity variations ($\frac{\Delta v}{v}$)

In Figs 3(a) and (d), the plots depict $\frac{\Delta v}{v}$ for both frequency bands in conjunction with temperature. Seasonal variations in $\frac{\Delta v}{v}$ are

Downloaded from https://academic.oup.com/gji/article/240/1/779/7905064 by Milak user on 17 January 2025

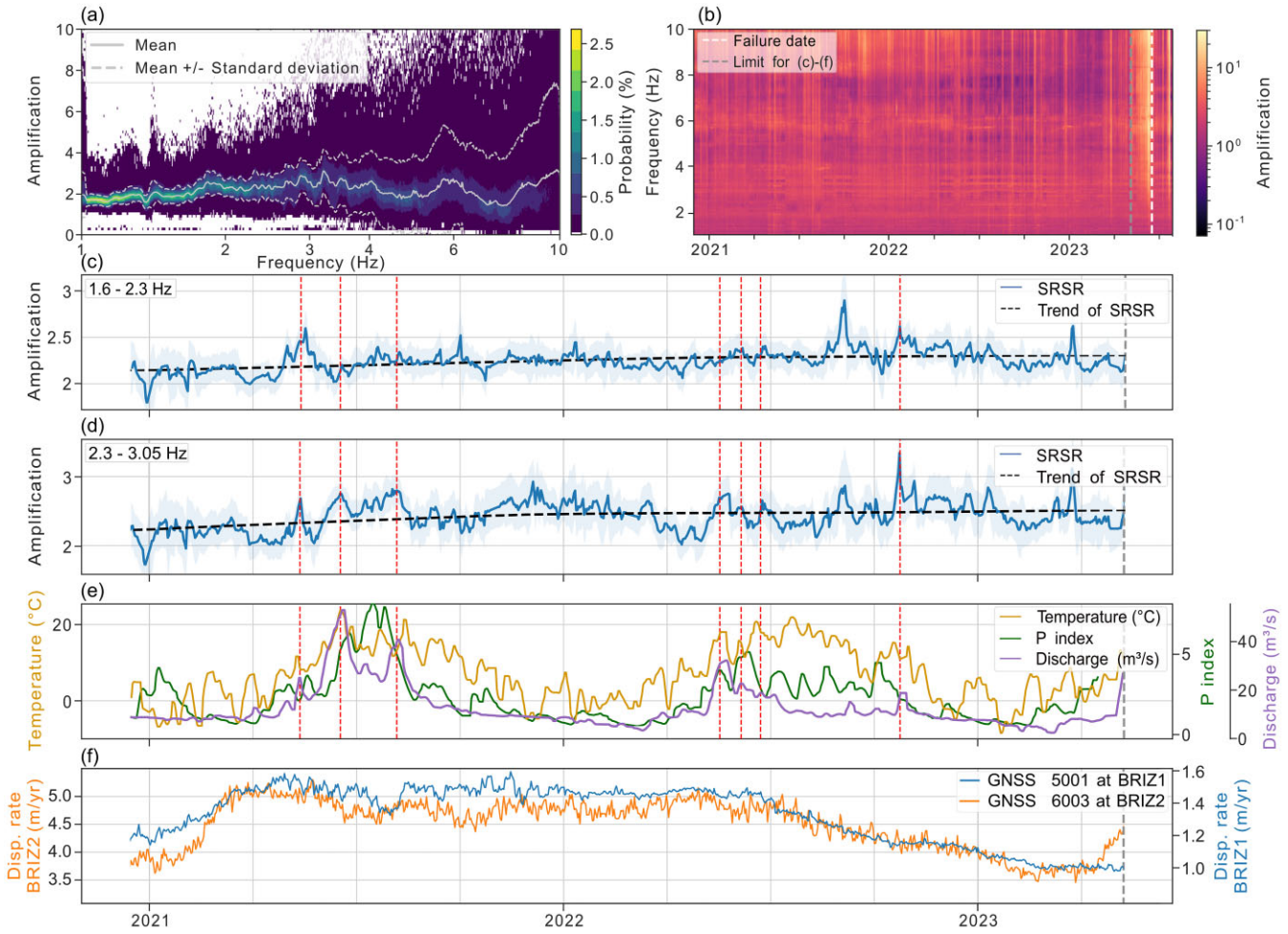


Figure 2. Results of SRSR and its relation with environmental parameters. (a) Probability density function of the daily amplification curve with the daily mean and standard deviation marked (b) Daily amplification spectrogram. (c) and (d) Daily median amplification for two frequency bands (1.6–2.3 Hz, 2.3–3.05 Hz). (e) Time series of environmental parameters. (f) Displacement rate of the instability.

discernible for both frequency bands (1.6–2.3 Hz and 2.3–3.05 Hz), exhibiting a seasonal variation of around ±0.5 per cent. The seasonal pattern of relative shear-wave variations closely follows the air temperature fluctuations. A deviation between temperature and $\frac{\Delta v}{v}$ arises during summer. Cross-plots of $\frac{\Delta v}{v}$ and temperature are shown in Figs 3(c) and (f), with data recorded during strong Albula discharge marked by a cross when the discharge is higher than 20 $m^3\,s^{-1}$. The Pearson correlation coefficient between temperature and relative seismic wave velocity variation is 0.4 and 0.68 for the first and second frequency bands, respectively. Figs 3(b) and (e) zoom in on a summer period (shaded rectangle in Figs 3(a) and (d)) for both frequency bands. Multiple ephemeral drops in wave velocity are observed, most starting after strong precipitation. The precipitation index in dark green, which accounts for previous precipitation, aligns well with the observed drop in velocity, for example, during August 2020. Some troughs, such as the first drop in June 2020, correlate poorly with precipitation but correspond to water input through snow melting. During these intervals, a reduction in the cross-correlation coefficient is noticeable, particularly pronounced in the second frequency band.

4.3 Resonance frequencies

The daily values of the first two resonance frequencies, which were picked with an automatic procedure (Häusler *et al.* 2024), are shown in Figs 4(a) and (b). To enhance result stability, a LOESS fit is applied. Both resonance frequencies display a noticeable linear decline throughout the monitoring period. The first resonance frequency peaks in late 2018, reaching approximately 2.1 Hz and gradually decreases to nearly 1.8 Hz by 2023. Similarly, the second resonance frequency, starting at 2.95 Hz in late 2018, decreases to almost 2.7 Hz in 2023. No distinct seasonal variation is observed over the monitoring period, and no clear and consistent relation with environmental parameters can be established.

4.4 Long-term trends

Figs 5(a) and (b) show the long-term trend of the three site response parameters as solid lines. Long-term trends are obtained by applying a local regression (LOESS method). Data are shown

Downloaded from https://academic.oup.com/gji/article/240/1/779/7905064 by Mlak user on 17 January 2025

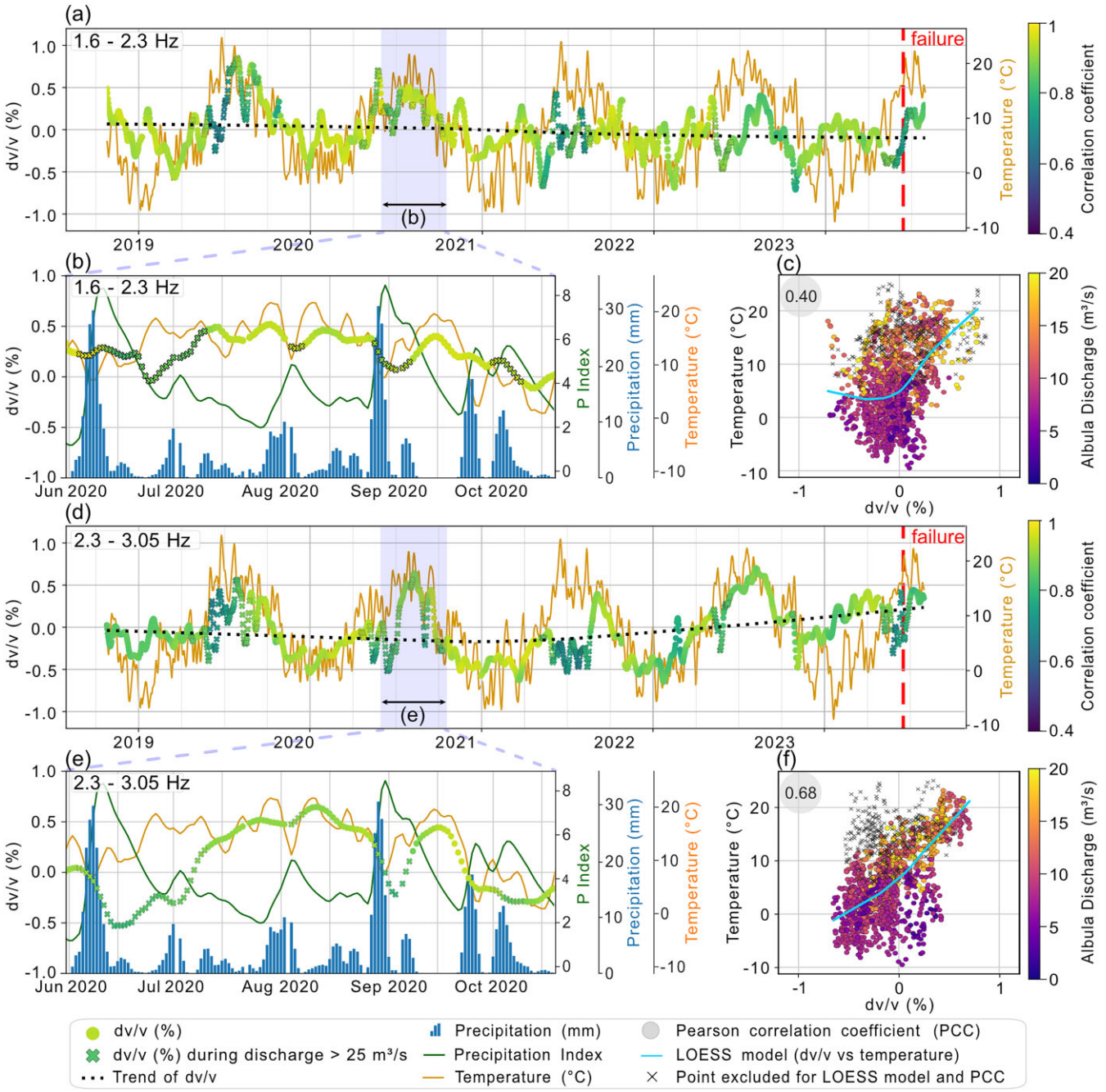


Figure 3. Relative seismic wave velocity variation results and its relation with environmental parameters. (a) and (d) show $\frac{\Delta v}{v}$ values for frequencies ranging from 1.6 to 2.3 Hz and 2.3 to 3.05 Hz, respectively. (b) and (e) show a zoom on the shaded area of subplots (a) and (d), respectively . (c) and (f) depict cross-plots between $\frac{\Delta v}{v}$ and the temperature excluding periods of large discharge (discharge over 20 $m^3\ s^{-1}$ are shown as crosses).

as scatter points with corresponding colours. The three time series for the first frequency band and the first resonance frequency show a weakening of the medium through an increase in amplification (in blue), a decrease in $\frac{\Delta v}{v}$ (in green) and a decrease in the first resonance frequency (in orange). For the second frequency bands and second resonance frequency, $\frac{\Delta v}{v}$ is increasing over time after an initial decrease, while the resonance frequency is decreasing and an amplification increase can be observed.

5 DISCUSSION

First, we discuss the (non)-observation of seasonal variations in site response, then the difference in the long-term trend of the three site-response parameters, and compare $\frac{\Delta v}{v}$ with other methods to acquire the seismic wave velocity variation. Finally, we briefly discuss the failure event of 2023 June 15.

Previous studies have established a correlation between resonance frequency and $\frac{\Delta v}{v}$, both exhibiting seasonal variations that

Downloaded from https://academic.oup.com/gji/article/240/1/779/7905064 by Mlak user on 17 January 2025

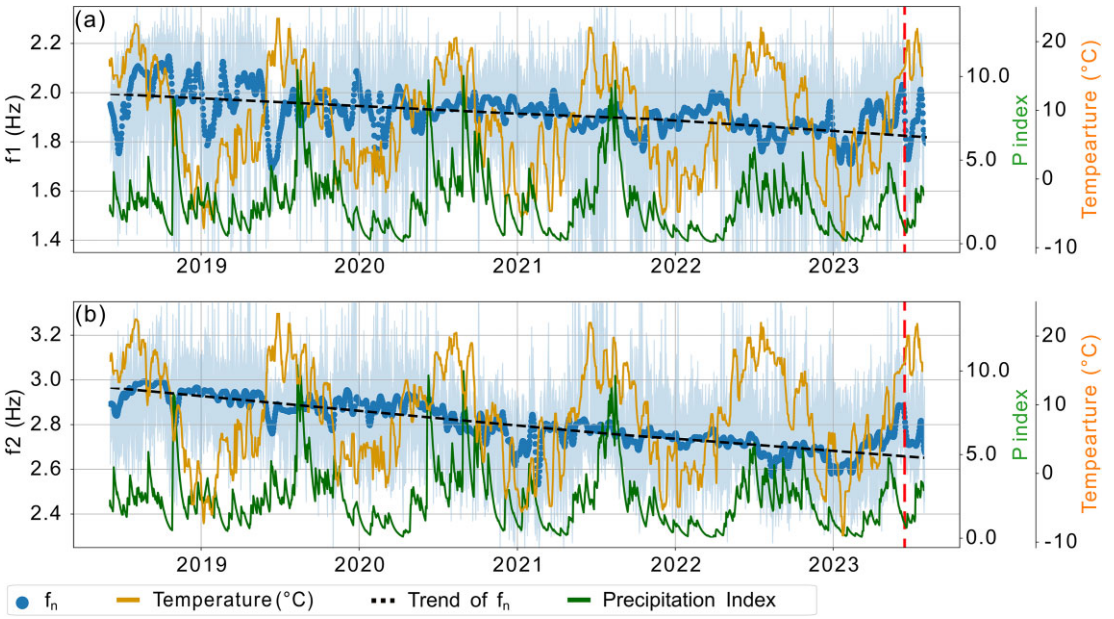


Figure 4. Time series of the first two resonance frequencies temperature and precipitation index plotted. The dots show the first (a) and second resonance frequency (b) with the standard deviation shown as a shaded area. LOESS method is applied to acquire the trend of resonance frequency. The vertical dashed line is the day of the failure of the Insel.

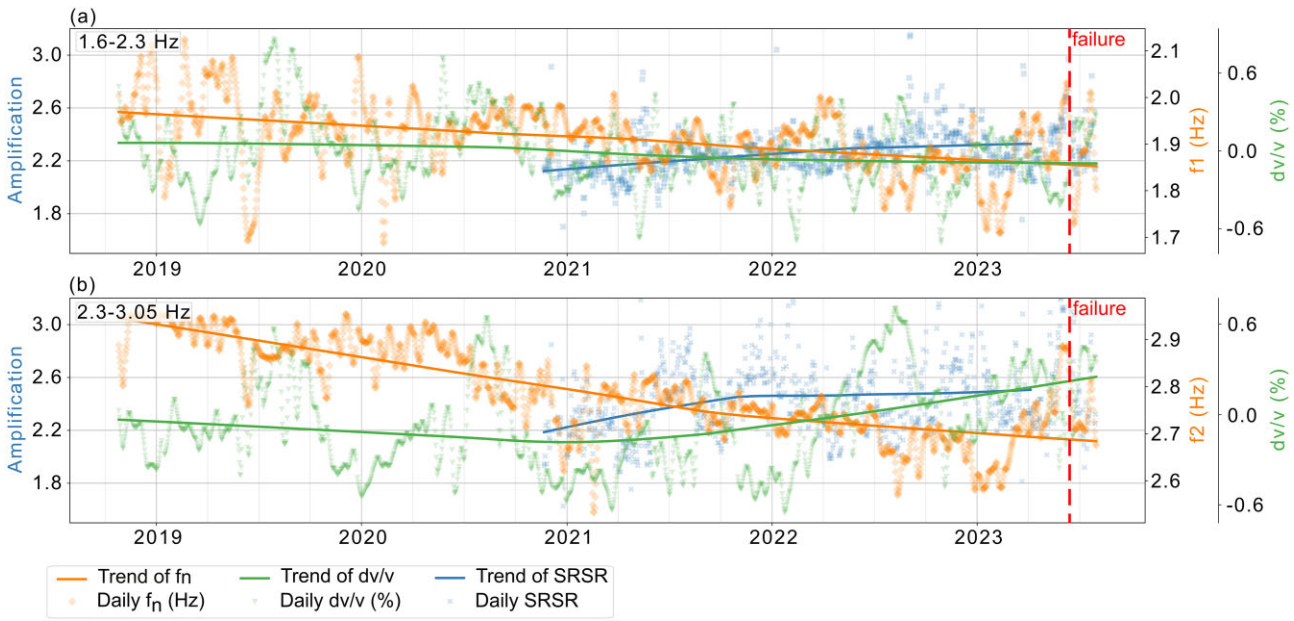


Figure 5. Long-term trend evolution of the three site-response parameters. The scatter points represent the daily data. (a) shows results for the first frequency band (1.6–2.3 Hz) and (b) for the second frequency band (2.3–3.05 Hz).

lagged the air temperature variations (e.g. Colombero *et al.* 2018; Valentin 2018). In these studies, site responses exhibited a lag relative to temperature changes, with delays from less than one day and two months, respectively. In our study, we could only identify distinct seasonal variations in seismic wave velocity. Borehole temperature monitoring over several months indicated that temperature penetration remains superficial, affecting only the top 30 m (cf. borehole KB9 in fig. 2 of Figi *et al.* 2022). Hence, it is likely that $\frac{\Delta v}{v}$ variations related to temperature changes depend on the shallow subsurface (other effects may trigger deeper changes). To support this statement, we conducted a depth sensitivity analysis. The results showed that surface waves are likely sensitive to the first 10–30 m of the subsurface using a hypothetical velocity profile (see Figs S5 and S6 of the Supporting Information). The other two site-response parameters may be linked to deeper structures, thus exhibiting different responses to environmental parameters. Häusler *et al.* (2022) interpreted that the first resonance frequency is sensitive to one large unstable volume, while the second

Downloaded from https://academic.oup.com/gji/article/240/1/779/7905064 by Milak user on 17 January 2025

resonance frequency is sensitive to a smaller subvolume near the station BRIZ2. We may also experience method limitations. As shown by Häusler *et al.* (2022), there was a clear correlation between absolute amplification and past precipitation at this site. In this study, we considered relative amplification using SRSR and did not find a clear correlation with environmental parameters. If the reference and site response are similar due to past precipitation, the relative amplification values may remain constant, while absolute amplification does not. Although the proximity of stations is a pre-requisite of SRSR to eliminate source and path effects, it may also eliminate responses due to environmental effects, resulting in a relative amplification that appears to be constant while the absolute amplification varies. Based on the results of the depth-sensitivity of $\frac{\Delta v}{v}$, we computed it for a lower frequency band (1.3–1.45 Hz) and found that $\frac{\Delta v}{v}$ for this frequency band do not show seasonal variation (no correlation with temperature) and exhibits a similar decay as the resonance frequency over the years (see Fig. S7 of the Supporting Information). So, the discrepancy between the different site-response parameters may be explained by method limitations (e.g. *relative* amplification) and/or by different depth/compartment sensitivities of the methods.

We computed $\frac{\Delta v}{v}$ using the cross-correlation between the reference and the site, utilizing *MSNoise* (Lecocq *et al.* 2014). Additionally, we computed the $\frac{\Delta v}{v}$ of the reference site BRIZ1 using a single-station approach. The three different $\frac{\Delta v}{v}$ curves showed a strong match when similar parameters were used (Fig. 6). This consistency suggests that $\frac{\Delta v}{v}$ is primarily influenced by shallow subsurface effects rather than deeper structural changes in the instability, as this site-response parameter is similar. As illustrated in Fig. 6(b), $\frac{\Delta v}{v}$ lags behind temperature by a few days. According to Colombero *et al.* (2021), this lag implies that rising temperatures may cause thermal dilation, leading to the closure of fractures and microcracks and increasing fracture contact stiffness. Other factors can drive the observed changes in $\frac{\Delta v}{v}$, such as the water content of the instability (e.g. Mainsant *et al.* 2012). We computed synthetic $\frac{\Delta v}{v}$ based on precipitation and discharge data following the methodologies in Barajas *et al.* (2021) and Delouche & Stehly (2023) as the water content of the instability can drive the variations in $\frac{\Delta v}{v}$. The synthetic results closely match the observed $\frac{\Delta v}{v}$ indicating that part of the $\frac{\Delta v}{v}$ variations can be attributed to changes in water content within the instability (see Figs S8 and S9 of the Supporting Information). To prove the used method detailed in the supplementary data, we also computed this synthetic $\frac{\Delta v}{v}$ for a stable rock site in Switzerland located nearby [DAVOX, data from Swiss Seismological Service (SED) at ETH Zurich (1983)] and found a good correlation between synthetic and observed $\frac{\Delta v}{v}$ (Fig. S8 (b), Supporting Information). After removing the effect of the water content on the observed $\frac{\Delta v}{v}$, it still correlates strongly with temperature and hydrological parameters. The variations of $\frac{\Delta v}{v}$ also correlate with the power of ambient vibrations, as shown in Figs S10 (a) and (b) of the Supporting Information, which could be due to spatiotemporal variations in noise sources affecting the results. Despite this, Fig. S10(c) of the Supporting Information shows that $\frac{\Delta v}{v}$ is ahead of the changes in power by several days, suggesting that these noise sources do not significantly drive the $\frac{\Delta v}{v}$ results. We also found no differences when using only night-time data to compute $\frac{\Delta v}{v}$, indicating that anthropogenic noise does not impact the stability of the BRIZ2 results. This suggests that temperature is likely the primary driver of the observed $\frac{\Delta v}{v}$, with rainfall and snowmelt playing a secondary role by temporarily decreasing $\frac{\Delta v}{v}$. The water content within the instability may also contribute to the00 variations.

Over the years, the first and second frequency bands have shown increased site amplification associated with decreased resonance frequency. The observed trends may be signs of an ongoing structural weakening and softening of the upper part of the instability. We suppose that the repeated effect of sliding, heavy precipitation and temperature variation are responsible for these observed trends through gradual damage accumulation. Nevertheless, we should not overlook changes in environmental parameters over the years that may influence site-response parameters. We observed a significant decrease in Albula discharge, which may act as a proxy of the water content of the instability. According to the Federal Office for Environment (FOEN), the discharge decreased from a monthly average of 18.6 $m^3\,s^{-1}$ in 2019 to 11.4 $m^3\,s^{-1}$ in 2022. Water content has the opposite effect as temperature for the different site response parameters (e.g. Colombero *et al.* 2021). Such a decrease in the water content over the years may create, thus, an increase in resonance frequency, $\frac{\Delta v}{v}$, and a decrease in amplification, which is not the case here. So, the observed weakening may be somewhat balanced by a dryer medium. Other environmental parameters stayed constant over the years.

Fig. S11 of the Supporting Information shows $\frac{\Delta v}{v}$ computed for a stable rock site in the same region for the station DAVOX (WGS84: 46.7805, 9.87952, elevation: 1830 m in July 2002) located near Davos (GR). $\frac{\Delta v}{v}$ for site DAVOX exhibits similar amplitude of seasonal variations as in BRIZ2 and BRIZ1, which are also in the range of other studies. Following the empirical law of Le Breton *et al.* (2021), we would expect $\sim$ 0.4 to 0.5 per cent of yearly amplitude variation in $\frac{\Delta v}{v}$. Contrary to our expectations, results show a continuous decrease of $\frac{\Delta v}{v}$ over the studied period, probably linked with changes in the water content of the site (Fig. S8, Supporting Information). For this reason, we do not give much weight to the observed long-term trend of $\frac{\Delta v}{v}$. Furthermore, as mentioned, this method for this site is likely mainly sensitive to shallow subsurface and not deeper structures.

In the literature, it has been demonstrated that $\frac{\Delta v}{v}$ and the resonance frequency may be potential early warning indicators for slope failures. Prior research, such as that conducted by Mainsant *et al.* (2012), has illustrated a decline in relative seismic wave velocity preceding the failure of a clayey landslide. Similarly, Lévy *et al.* (2010) observed a reduction in resonance frequency preceding a collapse. During our monitoring period in Brienz/Brinzauls, a part of the instability, the 'Insel,' collapsed on 2023 June 15. Our study did not yield compelling evidence of precursory signals in the different site-response parameters. The observed increase in relative site amplification post-April 2023 can be attributed to ambient vibrations originating from the acceleration of the 'Insel' compartment. The automatic picking of the resonance frequencies was strongly affected by internal seismic events due to sliding and rock fall. Lastly, $\frac{\Delta v}{v}$ did not show clear precursory signs of failure. Drops in $\frac{\Delta v}{v}$ in summer 2023 with a similar magnitude as the previous years were observed, which may be primarily due to the influence of hydrological effects (Figs 3 (a) and (c)).

6 CONCLUSION

This study compares three site-response parameters and their correlation with environmental factors at the Brienz/Brinzauls slope instability. The results suggest that changes in relative seismic wave velocity ($\frac{\Delta v}{v}$) are primarily controlled by thermomechanical effects. Temperature monitoring within a borehole shows that temperature fluctuations impact the first tens of metres of the unstable zone (Fig.

Downloaded from https://academic.oup.com/gji/article/240/1/779/7905064 by Milak user on 17 January 2025

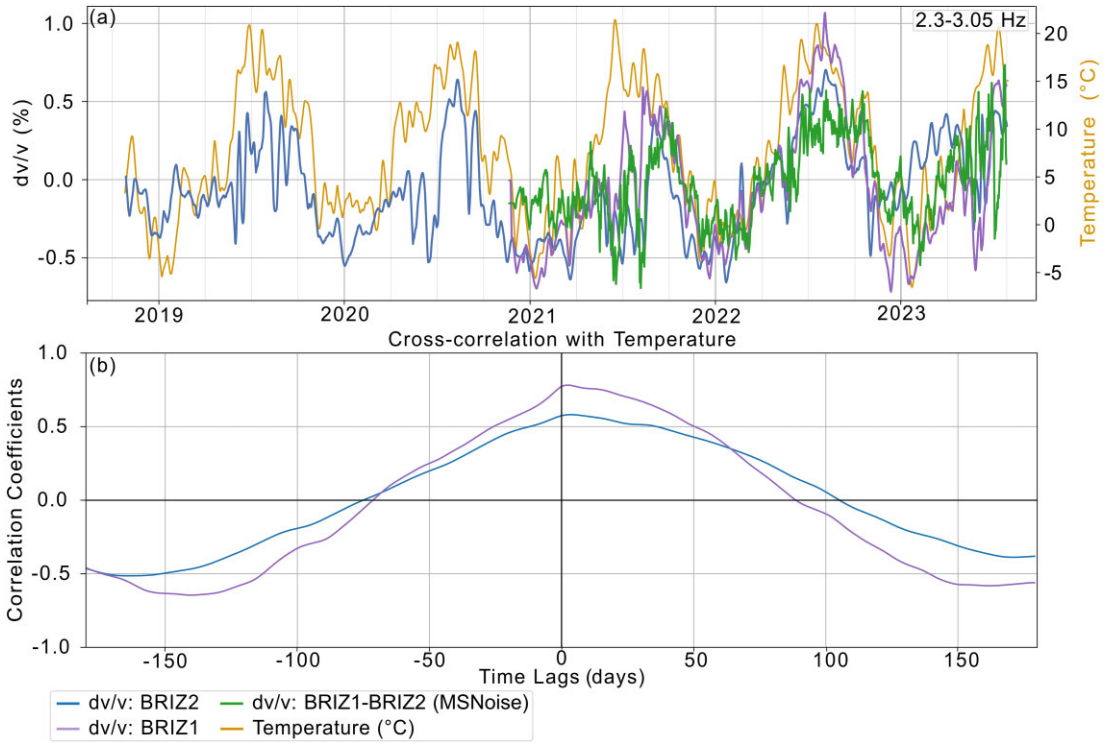


Figure 6. Comparison of different $\frac{\Delta v}{v}$ and time lag cross-correlation. (a) depicts time series of various $\frac{\Delta v}{v}$ results for frequencies between 2.3 and 3.05 Hz. (b) displays the correlation coefficient between the relative change in seismic velocity ($\frac{\Delta v}{v}$) and temperature over various time lags. The colours correspond to the colour of the panel (a). Positive time lags indicate that the air temperature variations happen before the $\frac{\Delta v}{v}$ or, in other words, that temperature may influence $\frac{\Delta v}{v}$.

2 of Figi *et al.* 2022), indicating that $\frac{\Delta v}{v}$ is sensitive to shallow subsurface conditions at this location. Rainfall and snow melt exert a secondary influence, with reductions in seismic wave velocity observed following these events, reaching up to 0.5 per cent. All the variations linked with environmental parameters are reversible. No long-term changes of $\frac{\Delta v}{v}$ were observed. In contrast, site amplification and resonance frequencies showed no substantial seasonal variation or consistent correlation with environmental factors. This may be due to methodological limitations (e.g. relative amplification smoothing out variations) and differences in sensitivities to various depths or structural compartments. Additionally, over time, we observed an increase in site amplification and a decrease in the first and second resonance frequencies, which may indicate progressive structural weakening. No gradual damage accumulation linked with environmental parameters can be established. As $\frac{\Delta v}{v}$ is mainly sensitive to the shallow subsurface, it may not be a suitable monitoring tool for this site and the frequencies we used. In contrast, monitoring resonance frequency may be best suited for this site as it showed a strong non-reversible decrease over time. Tracking site amplification may also be suitable, although it requires two stations.

AUTHOR CONTRIBUTIONS

FG and DF proposed the topic and conceived and designed the study. MHa and MHo supported XB in obtaining the different data. XB processed the data, carried out the data analysis and wrote the first draft of the manuscript. All the authors helped to interpret the results and write the final manuscript. All authors have read and approved the final manuscript.

CONFLICT OF INTEREST

The authors declare that they have no competing interests.

ACKNOWLEDGMENTS

This research was funded by the projects '4D seismic response and slope failure' Swiss National Science Foundation SNF (200021E 177586), 'Skyfall' ETHZ 0–20361–17, 'Quantification of the seismic response of instable slopes and its time variability: an important indicator for potential mass movements' SNF 200020_214916 and 'Erkennung, Charakterisierung und Überwachung von Instabilitäten mit seismischen Technologien' Swiss Federal Office for the Environment FOEN 00.5032.PZ / EC049A5A7. We thank the commune Albula/Alvra for their collaboration, shared data and unrestricted access to the site.

SUPPORTING INFORMATION

Supplementary data are available at *GJIRAS* online.

Figure S1. Amplification curve for both seismic stations.
Figure S2. Station location.
Figure S3. Correlogram of daily cross-correlation for BRIZ2.
Figure S4. Correlogram of daily cross-correlation for BRIZ1.
Figure S5. Hypothetical 1-D velocity model.
Figure S6. Sensitivity of surface waves.
Figure S7. d*v*/*v* for a lower frequency band.
Figure S8. Synthetic d*v*/*v* from precipitation and discharge data.
Figure S9. Subtracting of synthetic d*v*/*v* from observed d*v*/*v*.
Figure S10. d*v*/*v* and power.

Downloaded from https://academic.oup.com/gji/article/240/1/779/7905064 by Mlak user on 17 January 2025

Figure S11. d*v*/*v* for a stable rock site.

Please note: Oxford University Press is not responsible for the content or functionality of any supporting materials supplied by the authors. Any queries (other than missing material) should be directed to the corresponding author for the paper.

DATA AVAILABILITY

The data supporting this study's findings are available in https://doi.org/10.3929/ethz-b-000671357 for the seismic station BRIZ2 and in https://doi.org/10.3929/ethz-b-000677205 for the seismic station BRIZ1.

REFERENCES

Amitrano, D., Gaffet, S., Malet, J.-P. & Maquaire, O., 2007. Understanding mudslides through micro-seismic monitoring: the Super-Sauze (South-East French Alps) case study, *Bull. Soc. Géolog. France,* **178**(2), 149–157.

Barajas, A., Poli, P., D'Agostino, N., Margerin, L. & Campillo, M., 2021. Separation of Poroelastic and Elastic Processes of an Aquifer From Tectonic Phenomena Using Geodetic, Seismic, and Meteorological Data in the Pollino Region, Italy, *Geochem. Geophys. Geosyst.,* **22**(11), e2021GC009742, doi:10.1029/2021GC009742.

Bertello, L., Berti, M., Castellaro, S. & Squarzoni, G., 2018. Dynamics of an active earthflow inferred from surface wave monitoring, *J. geophys. Res.: Earth Surface,* **123**(8), 1811–1834.

Bessette-Kirton, E., Moore, J., Geimer, P.R., Finnegan, R., Häusler, M. & Dzubay, A., 2022. Structural characterization of a toppling rock slab from array-based ambient vibration measurements and numerical modal analysis, *J. geophys. Res.: Earth Surface,* **127**(8), e2022JF006679, doi:10.1029/2022JF006679.

Bontemps, N., Lacroix, P., Larose, E., Jara, J. & Taipe, E., 2020. Rain and small earthquakes maintain a slow-moving landslide in a persistent critical state, *Nat. Commun.,* **11**(1), 1–10.

Borcherdt, R.D., 1970. Effects of local geology on ground motion near San Francisco Bay, *Bull. seism. Soc. Am.,* **60**(1), 29–61.

Bottelin, P. *et al.*, 2013a. Spectral analysis of prone-to-fall rock compartments using ambient vibrations, *J. Environ. Eng. Geophys.,* **18**(4), 205–217.

Bottelin, P., Levy, C., Baillet, L., Jongmans, D. & Gueguen, P., 2013b. Modal and thermal analysis of Les Arches unstable rock column (Vercors massif, French Alps), *Geophys. J. Int.,* **194**(2), 849–858.

Bottelin, P., Mainsant, G., Jongmans, D., Baillet, L., Larose, E., Chambon, G. & Hantz, D., 2017. Suivi temporel de mouvements gravitaires: apport des vibrations sismiques ambiantes, *Rev. Franç. Géotechn.,* **152,** 1, doi:10.1051/geotech/2017011.

Brincker, R., Ventura, C.E. & Andersen, P., 2001. Damping estimation by frequency domain decomposition, in *Proceedings of IMAC 19: A conference on structural dynamics: Februar 5-8, 2001, Hyatt Orlando, Kissimmee, Florida, 2001,* Society for Experimental Mechanics, Bethel, pp. 698–703.

BTG (Büro für Technische Geologie AG), 2021. *Technical report No. 5897-13: Rutschung Brienz/Brinzauls GR, Geologische Detailuntersuchungen 2018 bis 2021, Sondierbohrungen. Geological report*. BTG Büro für Technische Geologie AG.

Burjánek, J., Gischig, V., Moore, J.R. & Fäh, D., 2018. Ambient vibration characterization and monitoring of a rock slope close to collapse, *Geophys. J. Int.,* **212**(1), 297–310.

Chen, W.-F. & Lui, E.M., 2005. *Handbook of Structural Engineering,* CRC Press: Boca Raton, Florida, USA.

Cleveland, W.S., 1979. Robust locally weighted regression and smoothing scatterplots, *J. Am. Stat. Assoc.,* **74**(368), 829–836.

Cohen, I., Huang, Y., Chen, J., Benesty, J., Benesty, J., Chen, J., Huang, Y. & Cohen, I., 2009. Pearson correlation coefficient, in *Noise Reduction in Speech Processing, Vol. 2,* pp. 1–4, Springer.

Colombero, C., Baillet, L., Comina, C., Jongmans, D., Larose, E., Valentin, J. & Vinciguerra, S., 2018. Integration of ambient seismic noise monitoring, displacement and meteorological measurements to infer the temperature-controlled long-term evolution of a complex prone-to-fall cliff, *Geophys. J. Int.,* **213**(3), 1876–1897.

Colombero, C., Jongmans, D., Fiolleau, S., Valentin, J., Baillet, L. & Bièvre, G., 2021. Seismic noise parameters as indicators of reversible modifications in slope stability: a review, *Surv. Geophys.,* **42,** 339–375.

Confédération Suisse, 2020. Adaptation aux changements climatiques en Suisse. Plan d'action 2020–2025. Le Conseil Fédéral: Berne, p. 164.

De Plaen, R.S., Lecocq, T., Caudron, C., Ferrazzini, V. & Francis, O., 2016. Single-station monitoring of volcanoes using seismic ambient noise, *Geophys. Res. Lett.,* **43**(16), 8511–8518.

Delouche, E. & Stehly, L., 2023. Seasonal seismic velocity variations measured using seismic noise autocorrelations to monitor the dynamic of aquifers in Greece, *J. geophys. Res.: Solid Earth,* **128,** doi:10.1029/2023JB026759.

Edwards, B., Michel, C., Poggi, V. & Fäh, D., 2013. Determination of site amplification from regional seismicity: Application to the Swiss National Seismic Networks, *Seism. Res. Lett.,* **84**(4), 611–621.

Figi, D., Thöny, R., Breitenmoser, T., Brunold, F. & Schwestermann, T., 2022. Rutschung Brienz/Brinzauls (GR): Geologisch-kinematisches und hydrogeologisches Model, *Swiss Bull. angew. Geol.,* **27**(2), 17–34, https://btgeo.ch/images/BTG_public/Publikationen-PDF/paper-brienz.pdf.

Finlayson, B. & Statham, I., 1980. *Hillslope analysis,* Butterworth-Heinemann: London, UK.

Fiolleau, S., Jongmans, D., Bièvre, G., Chambon, G., Baillet, L. & Vial, B., 2020. Seismic characterization of a clay-block rupture in Harmalière landslide, French Western Alps, *Geophys. J. Int.,* **221**(3), 1777–1788.

Geimer, P.R., Finnegan, R. & Moore, J.R., 2022. Meteorological controls on reversible resonance changes in Natural Rock Arches, *J. geophys. Res.: Earth Surface,* **127**(10), doi:10.1029/2022JF006734.

Gischig, V.S., Eberhardt, E., Moore, J.R. & Hungr, O., 2015. On the seismic response of deep-seated rock slope instabilities—Insights from numerical modeling, *Eng. Geol.,* **193,** 1–18.

Guillemot, A., Helmstetter, A.,,, Baillet, L., Garambois, S., Mayoraz, R. & Delaloye, R., 2020. Seismic monitoring in the Gugla rock glacier (Switzerland): ambient noise correlation, microseismicity and modelling, *Geophys. J. Int.,* **221**(3), 1719–1735.

Gunzburger, Y., Merrien-Soukatchoff, V. & Guglielmi, Y., 2005. Influence of daily surface temperature fluctuations on rock slope stability: case study of the Rochers de Valabres slope (France), *Int. J. Rock Mech. Mining Sci.,* **42**(3), 331–349.

Häusler, M., 2021. On the Dynamic Response of Unstable Rock Slopes: Characterization, monitoring, and modeling based on ambient vibration data, Ph.D. thesis, ETH Zurich.

Häusler, M., Gischig, V., Thöny, R., Glueer, F. & Fäh, D., 2022. Monitoring the changing seismic site response of a fast-moving rockslide (Brienz/Brinzauls, Switzerland), *Geophys. J. Int.,* **229**(1), 299–310.

Häusler, M., Glueer, F. & Fäh, D., 2024. The changing seismic site response of the Brienz/Brinzauls rock slope instability: insights from 5 years of monitoring before, during and after a partial collapse in June 2023, *Progr. Landslide Res. Technol.,* **3**(2), 559, doi:10.1093/gji/ggab473.

Häusler, M., Michel, C., Burjánek, J. & Fäh, D., 2019. Fracture network imaging on rock slope instabilities using resonance mode analysis, *Geophys. Res. Lett.,* **46**(12), 6497–6506.

Häusler, M., Michel, C., Burjanek, J. & Fäh, D., 2021. Monitoring the Preonzo rock slope instability using resonance mode analysis, *J. geophys. Res.: Earth Surface,* **126**(4), doi:10.1029/2020JF005709.

Heim, A., 1932. *Bergsturz und menschenleben,* **77**. Beiblatt zur Vierteljahrsschrift der Naturforschenden Gesellschaft in Zürich: Zürich, Switzerland.

Downloaded from https://academic.oup.com/gji/article/240/1/779/7905064 by Milak user on 17 January 2025

Helmstetter, A. & Garambois, S., 2010. Seismic monitoring of Séchilienne rockslide (French Alps): Analysis of seismic signals and their correlation with rainfalls, *J. geophys. Res.: Earth Surface,* **115**(F3), doi:10.1029/2009JF001532.

Hillers, G., Ben-Zion, Y., Campillo, M. & Zigone, D., 2015. Seasonal variations of seismic velocities in the San Jacinto fault area observed with ambient seismic noise, *Geophys. J. Int.,* **202**(2), 920–932.

Hillers, G., Campillo, M. & Ma, K.-F., 2014. Seismic velocity variations at TCDP are controlled by MJO driven precipitation pattern and high fluid discharge properties, *Earth planet. Sci. Lett.,* **391,** 121–127.

Hobiger, M., Wegler, U., Shiomi, K. & Nakahara, H., 2014. Single-station cross-correlation analysis of ambient seismic noise: application to stations in the surroundings of the 2008 Iwate-Miyagi Nairiku earthquake, *Geophys. J. Int.,* **198**(1), 90–109.

Intercantonal Measurement and Information System IMIS. 2023. IMIS measuring network. *EnviDat*. https://www.doi.org/10.16904/envidat.406.

Jia, Y., Jiang, T., Liu, H. *et al.*, 2021. Stability evaluation model of toppling unstable rock based on natural vibration frequency, *J. appl. Sci. Eng.,* **24**(2), 177–184.

Jia, Y., Song, G., Jiang, T., Yu, G., Liu, H. & Pan, X., 2022. Buried depth calculation of the slope of the unstable rock based on natural vibration frequency, *Front. Earth Sci.,* **10,** doi:10.3389/feart.2022.929825.

Julian, M. & Anthony, E., 1996. Aspects of landslide activity in the Mercantour Massif and the French Riviera, southeastern France, *Geomorphology,* **15**(3-4), 275–289.

Kasımzade, A.A., Tuhta, S., Günday, F. & Aydın, H., 2019. Investigation of Modal Parameters on Steel Structure Using FDD from Ambient Vibration, in *8th International Steel Structures Symposium, Konya*.

Kleinbrod, U., Burjánek, J. & Fäh, D., 2019. Ambient vibration classification of unstable rock slopes: a systematic approach, *Eng. Geol.,* **249,** 198–217.

Kleinbrod, U., Burjánek, J., Hugentobler, M., Amann, F. & Fäh, D., 2017. A comparative study on seismic response of two unstable rock slopes within same tectonic setting but different activity level, *Geophys. J. Int.,* **211**(3), 1428–1448.

Krähenbühl, R. & Nänni, C., 2017. Ist das dorf Brienz-Brinzauls bergsturz gefährdet, *Swiss Bull. angew. Geol,* **22**(2), 33–47.

Larose, E. *et al.*, 2015. Environmental seismology: What can we learn on earth surface processes with ambient noise?, *J. appl. Geophys.,* **116,** 62–74.

Le Breton, M., Bontemps, N., Guillemot, A., Baillet, L. & Larose, É., 2021. Landslide monitoring using seismic ambient noise correlation: challenges and applications, *Earth-Science Rev.,* **216,** 103518, doi:10.1016/j.earscirev.2021.103518.

Lecocq, T., Caudron, C. & Brenguier, F., 2014. MSNoise, a python package for monitoring seismic velocity changes using ambient seismic noise, *Seism. Res. Lett.,* **85**(3), 715–726.

Lévy, C., Baillet, L., Jongmans, D., Mourot, P. & Hantz, D., 2010. Dynamic response of the Chamousset rock column (Western Alps, France), *J. geophys. Res.: Earth Surface,* **115**(F4), doi:10.1029/2009JF001606.

Loew, S., Huwiler, A., Schneider, S., Largiader, A., Naenni, C., Figi, D., Thoeny, R. & Josuran, M., 2023. *Summary of the 15 June 2023 Brienz/Brinzauls rockslide collapse in the Swiss Alps,* The Landslide Blog, AGU.

Mainsant, G., Larose, E., Brönnimann, C., Jongmans, D., Michoud, C. & Jaboyedoff, M., 2012. Ambient seismic noise monitoring of a clay landslide: Toward failure prediction, *J. geophys. Res.: Earth Surface,* **117**(F1), doi:10.1029/2011JF002159.

Meier, U., Shapiro, N.M. & Brenguier, F., 2010. Detecting seasonal variations in seismic velocities within Los Angeles basin from correlations of ambient seismic noise, *Geophys. J. Int.,* **181**(2), 985–996.

Niu, F., Silver, P.G., Daley, T.M., Cheng, X. & Majer, E.L., 2008. Preseismic velocity changes observed from active source monitoring at the Parkfield SAFOD drill site, *Nature,* **454**(7201), 204–208.

Obermann, A., Froment, B., Campillo, M., Larose, E., Planès, T., Valette, B., Chen, J. & Liu, Q., 2014. Seismic noise correlations to image structural and mechanical changes associated with the M_w 7.9 2008 Wenchuan earthquake, *J. geophys. Res.: Solid Earth,* **119**(4), 3155–3168.

Perron, V., Gélis, C., Froment, B., Hollender, F., Bard, P.-Y., Cultrera, G. & Cushing, E.M., 2018. Can broad-band earthquake site responses be predicted by the ambient noise spectral ratio? Insight from observations at two sedimentary basins, *Geophys. J. Int.,* **215**(2), 1442–1454.

Prieto, G., Parker, R., &, 2009. A fortran 90 library for multitaper spectrum analysis, *Comput. Geosci.,* **35**(8), 1701–1710.

Richter, T., Sens-Schönfelder, C., Kind, R. & Asch, G., 2014. Comprehensive observation and modeling of earthquake and temperature-related seismic velocity changes in northern Chile with passive image interferometry, *J. geophys. Res.: Solid Earth,* **119**(6), 4747–4765.

Schneider, M., Oestreicher, N., Ehrat, T. & Loew, S., 2023. Rockfall monitoring with a Doppler radar on an active rockslide complex in Brienz/Brinzauls (Switzerland), *Nat. Hazards Earth Syst. Sci.,* **23**(11), 3337–3354.

Swiss Seismological Service (SED) at ETH Zurich, 1983. National Seismic Networks of Switzerland, doi:10.12686/SED/NETWORKS/CH

Swiss Seismological Service (SED) At ETH Zurich, 2012. Temporary deployments in switzerland associated with landslides, doi:10.12686/SED/NETWORKS/XP.

Valentin, J., 2018. Suivi de glissements rocheux et de coulées dans les roches argileuses à partir de méthodes sismiques et photogrammétriques, Ph.D. thesis, Université Grenoble Alpes (ComUE).

Voisin, C., Garambois, S., Massey, C. & Brossier, R., 2016. Seismic noise monitoring of the water table in a deep-seated, slow-moving landslide, *Interpretation,* **4**(3), SJ67–SJ76.

Downloaded from https://academic.oup.com/gji/article/240/1/779/7905064 by Milak user on 17 January 2025

© The Author(s) 2024. Published by Oxford University Press on behalf of The Royal Astronomical Society. This is an Open Access article distributed under the terms of the Creative Commons Attribution License (https://creativecommons.org/licenses/by/4.0/), which permits unrestricted reuse, distribution, and reproduction in any medium, provided the original work is properly cited.